



# Solution processed thin films of Nb-doped TiO<sub>2</sub> nanoparticles as hole blocking layer for organic solar cells

Wonmok Lee<sup>a,\*</sup>, Incheol Kim<sup>a</sup>, Ilwoo Ok<sup>b</sup>, Dahee Ahn<sup>a</sup>, Hyunjung Lee<sup>c</sup>, Jin-Ho Kim<sup>d</sup>, Kyungkon Kim<sup>e,\*\*</sup>

<sup>a</sup> Department of Chemistry, Sejong University, Seoul 143-747, Republic of Korea

<sup>b</sup> Korea Institute of Science and Technology, Seoul 136-791, Republic of Korea

<sup>c</sup> School of Advanced Materials Engineering, Kookmin University, 861-1 Jeongneung-Dong, Seoul, Republic of Korea

<sup>d</sup> Korea Institute of Ceramic Engineering and Technology, Icheon, Gyeonggi 467-843, Republic of Korea

<sup>e</sup> Department of Chemistry, Ewha Womans University, Seoul 136-791, Republic of Korea

## ARTICLE INFO

Available online 10 December 2013

### Keywords:

Nb-doped TiO<sub>2</sub> nanoparticles  
Sol-gel method  
Organically modified  
Thin film  
Hole-blocking layer  
Organic hetero-junction solar cell

## ABSTRACT

In this study, Nb-doped TiO<sub>2</sub> nanoparticles were synthesized by sol-gel method with controlled doping ratios up to 6 mol%. Catalyzed by *p*-toluene sulfonic acid, alkoxide precursors of Ti and Ni were stabilized by acetylacetonate ligand, and converted to the organically modified nanoparticles which were well dispersible in alcohols. Transmission electron microscopy and X-ray diffraction measurements revealed that TiO<sub>2</sub> nanoparticle possesses anatase morphologies, and the doping ratios were confirmed by X-ray photoelectron spectroscopy. Uniform thin films of Nb-doped TiO<sub>2</sub> were obtained by spin coating dilute alcohol dispersions of Nb-doped nanoparticles. Ellipsometric characterizations were carried out for the as-coated film and the sintered film as well to characterize the indices of refraction, and atomic force microscopy showed subnanometer-scale roughness of Nb-doped films. Owing to the improved roughness via doping, Nb-doped TiO<sub>2</sub> thin films exhibited enhanced solar cell efficiencies when used as hole-blocking layer of organic hetero-junction solar cell.

© 2013 Elsevier B.V. All rights reserved.

## 1. Introduction

Due to worldwide increase of energy consumption, finding reliable sustainable energy sources are of great interest among researchers [1]. In the research field seeking for a suitable electric power source particularly toward portable devices, heterojunction organic solar cell (OSC) has been one of the hottest topics owing to the advantageous features such as light weight, flexibility, processing cost, etc. [2–8]. Compared to dye-sensitized solar cell, no requirement of liquid electrolyte in OSC can make it more suitable for flexible and wearable devices in which leakage is a crucial issue. However, relatively low photon to current conversion efficiency (PCE) of OSC is still an important challenge to be overcome. Many efforts have been devoted to improve energy conversion efficiency in OSC devices [9,10]. In OSC, electron-hole recombination at the interface between the electrodes and active layer is one of the most serious problems causing the efficiency decrease. Insertion of thin N-type inorganic layer such as TiO<sub>2</sub> can help diminish the charge recombination at the interface by selectively allowing electron passage while preventing hole transport. Moreover, it can increase a long-term stability of the photovoltaic cell by preventing it from passage of reactive species in air [11–21]. Recently, we have reported that the

organically modified TiO<sub>2</sub> nanoparticles can form a thin conformal interlayer within a tandem solar cell to improve long-term stability of the device [22]. By doping Nb or W within TiO<sub>2</sub> lattices, it is reported that the optical and electronic properties can be further improved while preserving the original crystalline structure owing to similar ionic sizes of Nb and Ti [18,20,21,23]. Zhang et al. reported that doping with metal cation in TiO<sub>2</sub> can also suppress charge recombination problem in OSC [23].

In this study, we synthesize the organically modified Nb-doped TiO<sub>2</sub> nanoparticles for wet-coating process via sol-gel method. Uniform thin films of the nanoparticles are prepared, and rigorously characterized. Consequently, thin films are applied as hole blocking layer (HBL) for OSC devices.

## 2. Experimental details

### 2.1. Sol-gel synthesis of Nb-doped TiO<sub>2</sub> nanoparticle

We modified the synthetic procedures of our recent report to obtain Nb-doped TiO<sub>2</sub> nanoparticle [24]. In a typical experiment, 5.006 g of acetyl acetone (AcAc) (Aldrich) was added in round bottom flask containing 34.06 g of 1-butanol (Duksan Chemical) with vigorous stirring. Subsequently, 17.018 g of Titanium n-butoxide (Aldrich) and Niobium n-butoxide (Alfa-aeser) of a desired molar ratio to Titanium precursor were slowly added, and then the solution turned bright yellow upon mixing. While maintaining the reactor temperature at 60 °C, 1.9022 g

\* Correspondence to: W. Lee, Department of Chemistry, Sejong University, Seoul, 143-747, Republic of Korea.

\*\* Correspondence to: K. Kim, Department of Chemistry, Ewha Womans University, Seoul, 136-791, Republic of Korea.

**Table 1**  
Characterization of Nb-doped TiO<sub>2</sub> nanoparticles.

Nb content in the feed	0%	3%	6%
Nb content (by XPS)	0%	2.5%	5.7%
Average particle size (by XRD)	2.8 ± 0.4 nm	2.4 ± 0.6 nm	1.8 ± 0.6 nm
Organic content (by TGA)	27%	25%	34%

of *p*-toluene sulfonic acid (Aldrich) dissolved in 9 g of deionized water was added dropwise to the precursor solution to conduct the sol-gel reaction for 24 h. The yellow product was precipitated in an excess amount of toluene, and the precipitate was subsequently centrifuged, washed with toluene, and vacuum dried [24].

## 2.2. Characterization of nanoparticles and thin films

For transmission electron microscopic (TEM) analysis of a Nb-doped TiO<sub>2</sub> nanoparticle, 10<sup>-3</sup> wt.% dispersion of a powder product in 1-butanol was cast on the carbon-coated Cu grid. After vacuum-drying at room temperature (r.t.), the nanoparticles were imaged by high resolution (HR) TEM (Tecnai F20, FEI). Overall crystalline structures and average particle size of the powder product were characterized using X-ray diffractometer (XRD, Rigaku D/Max-2500) with Cu-K radiation as light source. The beam size of XRD was 1.7 × 10 mm<sup>2</sup>, and the measurement was done within 10–80 deg angular range at 1 deg/min scan rate. Thermogravimetric analysis (TGA, Mettler-Toledo TGA/DSC1) was performed to determine organic contents in the powder product. For a TGA run, 20 mg of each vacuum-dried sample was put into an aluminum pan, and heated from r.t. to 600 °C under air with a heating rate of 10 °C/min. A thin film of Nb-doped TiO<sub>2</sub> nanoparticle was prepared by spin-coating 2 wt.% nanoparticle dispersion in 1-butanol at 1500 rpm on Si wafer which had been cleaned by Piranha solution prior to coating. The coated films were either vacuum-dried at 100 °C or sintered at 500 °C for 6 h. To quantify the doping ratio of Nb, X-ray photoelectron spectroscopy (XPS, Ulvac, PHI 5000 Versa Probe) data was obtained from a spin-coated sample on Si wafer using a focused X-ray beam from Al anode at 0–1000 eV scanned energy range with 1.0 eV steps for wide scan. Narrow scans were also carried out to better resolve each characteristic peak with 0.1 eV steps. And spectroscopic ellipsometer (NanoView, MF-1000) was used to characterize the refractive index (*n*), the extinction coefficient (*k*) and the thickness of a spin-coated film on Si wafer. An optical raw data of a film was obtained at a fixed angle of 70 deg, and then fitted by Tauc-Lorentz function to give *n* and *k* values of each film. Surface morphology and roughness of the coated film were analyzed by using tapping-mode atomic force microscopy (AFM) (Asylum). The sheet resistance was measured by a four-probe method at r.t. The probe head used was a 4-point cylindrical probe head (Jandel Eng. Ltd.). A direct current precision power source (Keithley 6220) and nanovoltmeter (Keithley 2182A) were used, and Ni (0.00081 Ω/sq) was used as reference.

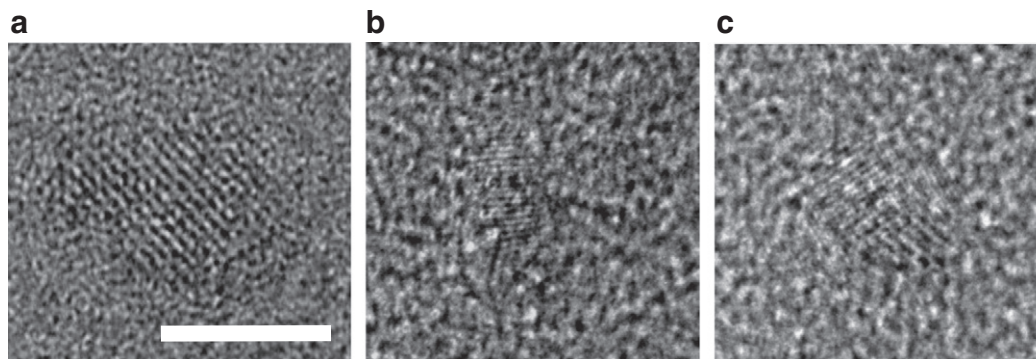


**Fig. 1.** HR-TEM images of (a) undoped TiO<sub>2</sub> nanoparticle, (b) 3%, and (c) 6% Nb-doped TiO<sub>2</sub> nanoparticles. Each nanoparticle appears to be irregular in shapes and with different crystalline facets. All the images show the same magnification. Scale bar represents 5 nm.

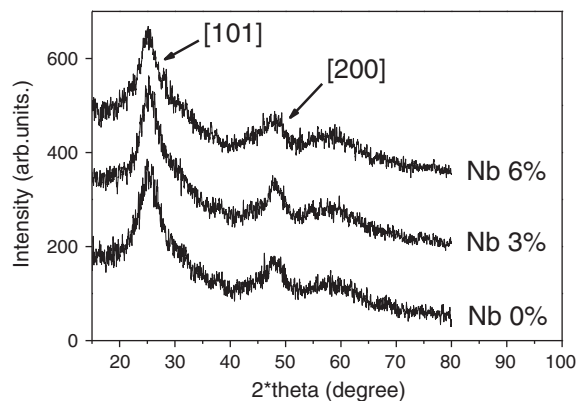


**Fig. 2.** Powder XRD data of undoped and Nb-doped TiO<sub>2</sub> nanoparticles. The full widths at half maximum of [101] and [200] anatase peaks for each sample were used for calculation of the average particle sizes.

## 2.3. Preparation of organic solar cell and performance test

Nb-doped TiO<sub>2</sub> nanoparticles developed in this study were tested as HBL for organic solar cell. Fabrication of a single cell was carried out in the glove box. First, 1:1 weight ratio of poly(3,4-ethylenedioxythiophene): poly(styrenesulfonate) dispersed in methanol was spin-coated on indium tin oxide (ITO) glass at 4000 rpm to form hole-transporting layer (HTL), followed by post-annealing at 155 °C for 20 min. Active layer was formed by spin-coating 1: 0.6 weight ratio of poly(3-hexylthiophene) (P3HT): 1-(3-methoxycarbonyl)propyl-1-phenyl [6,6]C<sub>61</sub> (PCBM) dissolved in chlorobenzene on HTL at 1000 rpm, and subsequently drying at 100 °C. And, 0.5 wt.% dispersion of Nb-doped TiO<sub>2</sub> nanoparticles in 1-butanol was filtered by 0.45 μm membrane disk filter twice, and spin-coated on the active layer. After annealing at 150 °C, 100 nm thick Al electrode was deposited using laser beam under vacuum condition of 2.67 × 10<sup>-3</sup> Pa. The single cell was then finally annealed using radiation heater at 155 °C for 10 min. Photocurrent-voltage characteristic of a single cell was carried out using Keithley model 2400 apparatus at AM 1.5G radiation condition [22].

## 3. Results and discussion

Surface modification of Nb-doped TiO<sub>2</sub> nanoparticles by AcAc ligand ensures thermodynamic stabilization between nanoparticles, thus the precipitated product can be redispersed in alcohol solvent by gentle agitation and heating (~60 °C) with up to 30 wt.% solid content [24]. Three different nanoparticle samples were prepared with respective Nb doping ratio of 0, 3, and 6 mol%. Heavier doping of Nb more than 10 mol% was also carried out, which appeared to be unsuccessful due to a relatively poor dispersibility in organic solvent. Since the

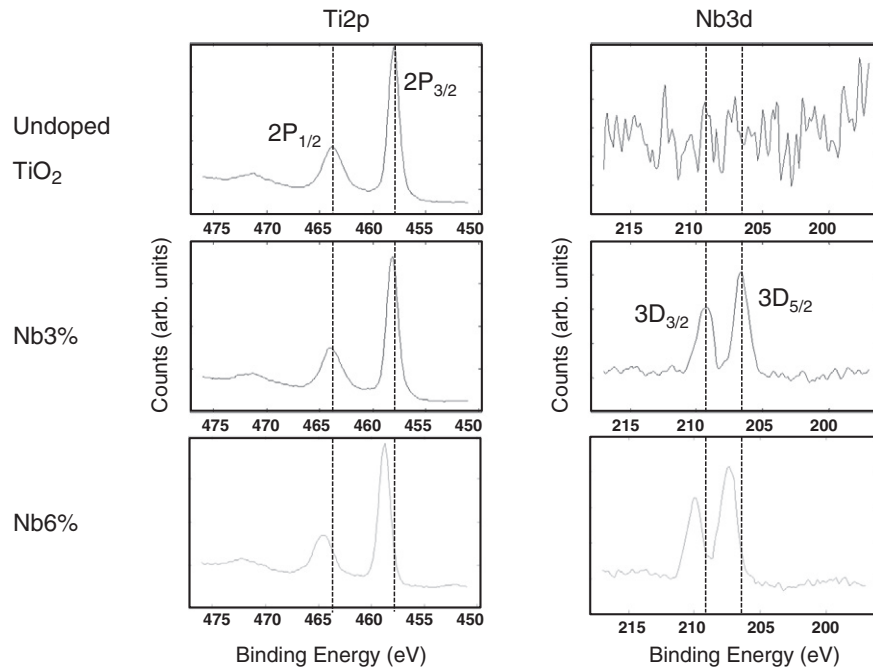


Fig. 3. XPS narrow scan spectra of the undoped and Nb-doped  $\text{TiO}_2$  samples showing Ti2p, and Nb3d doublet peaks originating from the different multiplicities.

nanoparticles were stabilized by organic AcAc ligands, HR-TEM images of each sample exhibited individual nanoparticle distributed on the carbon grid without agglomeration, although the visualization was not straightforward due to their small sizes. TGA analysis on the powder products revealed that every sample contained organic content more than 25 wt.% as summarized in Table 1. The surfaces of both undoped and doped  $\text{TiO}_2$  nanoparticles are stabilized by AcAc ligands coordinating to Ti metal, and thermal decomposition of organic components takes place during TGA to give us their amount originally included in the particles [24]. Fig. 1 shows the ellipsoidal shape of  $\text{TiO}_2$  nanocrystal, and nonspherically shaped Nb-doped nanoparticles showing the distinct crystalline facets. Owing to a weak contrast of  $\text{TiO}_2$  particles with carbon background in HR-TEM, nanoparticles smaller than 2 nm couldn't be images. Through powder XRD analysis as shown in Fig. 2, it was found that both bare and Nb-doped  $\text{TiO}_2$  crystal exhibited anatase phases, and incorporation of Nb precursor during the synthesis of  $\text{TiO}_2$  resulted in the decreased  $\text{TiO}_2$  particle size. For calculation of the average particle sizes, Scherrer analysis was applied to both [101] and [200] peaks of anatase  $\text{TiO}_2$  which appeared at 25.1 deg and 47.1 deg respectively. Owing to the broadness of XRD peaks, peak shifts or appearance of new peaks was hardly observable, and thus the inclusion of Nb oxide within  $\text{TiO}_2$  anatase crystal couldn't be traced by XRD. However, XPS analysis of the spin-coated samples on Si wafer apparently revealed the existence of Nb oxide, and the calculated Nb contents were confirmed to follow the Nb amount introduced in the feeds. (See Table 1) The corresponding narrow-scan XPS spectra of Ti2p and

Nb3d peaks are shown in Fig. 3. It is worthwhile to note that the peak for Nb3d<sub>5/2</sub> electron is located at 206.8 eV for the 3% Nb-doped sample and the peak shifts toward higher energy (207.6 eV) upon higher doping. Since the binding energies of Nb<sup>4+</sup> and Nb<sup>5+</sup> are located at 206 and 207.8 eV respectively, both oxidation states of Nb are supposed to exist in  $\text{TiO}_2$  matrix of our samples while they are dominantly in Nb<sup>5+</sup> form at 6% doping [25]. Therefore, we can assume that Nb<sub>2</sub>O<sub>5</sub> is a major doped component within  $\text{TiO}_2$  matrix, while coexisting with small amount of NbO<sub>2</sub> [26]. In addition, wide-scan XPS revealed the existence of small amount of sulfur which should be originating from the p-toluene sulfonic acid residue, which will add up to the organic contents. Thin films of Nb-doped  $\text{TiO}_2$  nanoparticles were prepared by spin coating their dispersions in 1-butanol on Si substrates. Owing to the excellent dispersibilities of the nanoparticles in n-butanol as well as their small particle sizes, uniform thin films could be obtained. Sintering at 450 °C resulted in the reflective color change of thin films owing to the altered refractive indices and thicknesses. Thin film properties of Nb-doped  $\text{TiO}_2$  nanoparticles were characterized by ellipsometry and tapping-mode AFM, and the results are summarized in Table 2. As

Table 2

Characteristics of Nb-doped  $\text{TiO}_2$  thin films.

Nb content in $\text{TiO}_2$ films		0%	3%	6%
Refractive index <sup>a</sup>	As coated	1.81	1.79	1.79
	After sintering	1.97	2.03	2.05
Thickness <sup>a</sup>	As coated	75	78	88
	After sintering	48	53	48
Roughness <sup>b</sup> (nm)	As coated	1.10	0.53	0.76
	After sintering	0.56	0.49	0.36
Resistance <sup>c</sup> (KΩ/sq)	As coated	6.2 ± 0.3	7.7 ± 0.8	7.0 ± 0.5
	After sintering	6.2 ± 0.3	7.7 ± 0.8	7.0 ± 0.5

<sup>a</sup> Refractive indices (@ 500 nm) and thicknesses were measured by ellipsometry.

<sup>b</sup> Film roughnesses were measured by AFM.

<sup>c</sup> Film resistances were measured by four-probe method.

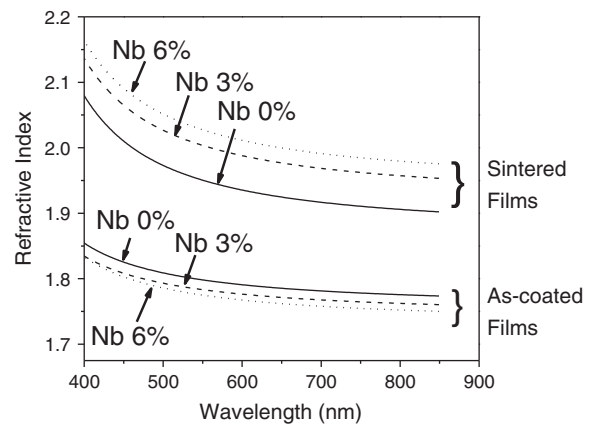


Fig. 4. Refractive indices of Nb-doped  $\text{TiO}_2$  films as a function of wavelength before and after sintering. Ellipsometry raw data were processed to obtain the spectroscopic refractive indices of the films. Substantial increases in all values are obvious resulting from thermal sintering of each film.

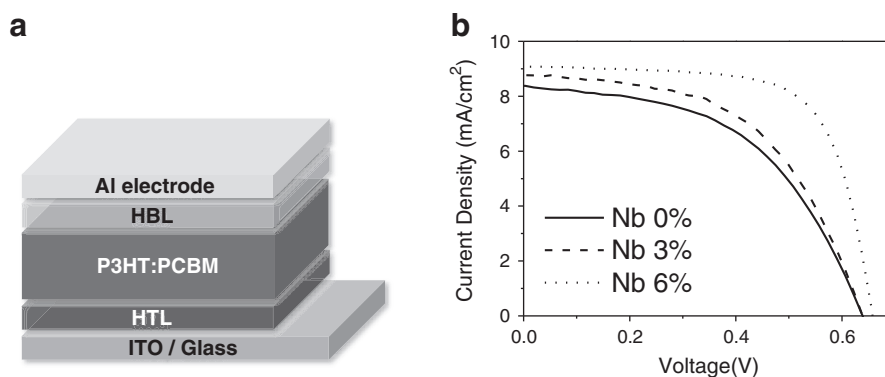


Fig. 5. (a) Illustration of OSC single cell with Nb-doped  $\text{TiO}_2$  as HBL in between active layer and ITO electrode. (b) I–V curve for the single cells.

shown in Fig. 4, refractive indices of the films showed a decreasing tendency with wavelength. Ellipsometric analysis revealed that the as-coated films have the refractive indices in the range of 1.78–1.81 at 500 nm wavelength of incident light which seem to be low for  $\text{TiO}_2$  films. However, those values are still substantial taking the high organic contents (25–35%) into account. A  $\text{TiO}_2$  film without doping showed the highest refractive index among others supposedly due to the large particle size. On the other hand, the refractive index sequence of the sintered films showed the reversed tendency compared with those of as-coated films. It is noteworthy that the removal of organic group by sintering rendered the film refractive index as high as 1.97–2.09 which shows more than 20% enhancement. More importantly, the undoped  $\text{TiO}_2$  film showed the lowest refractive index after sintering. It can be attributed to the removal of organic group, and also to the altered particle size during the sintering process. Nevertheless, a notable dependence of Nb doping ratio on the refractive indices of the films was hardly found. The ellipsometry also revealed a significant enhancement in extinction coefficients of each film (almost 5-fold) after sintering, while a noticeable dependence on Nb-doping couldn't be traced again. (Supporting data) Film thicknesses were measured to be in the range of 75–88 nm at the given concentration and spin rate, which have been decreased by ~30% upon sintering. Surface morphology and roughness of the coated films were characterized by tapping-mode AFM, from which very even surface without pinhole was imaged for every film with average roughness of 0.80 nm as shown in Table 2. Sintering has evidently decreased the average film roughness down to 0.47 nm again owing to the removal of organic ligand and thermal annealing effect as well. Average roughness sequence of the sintered films in Table 2 is in good accordance with the refractive index sequence shown in Fig. 4(b), where less rougher film exhibits higher index of refraction. The sheet resistance values of the sintered films measured by four-probe method shown in Table 2 indicate higher resistances in Nb-doped  $\text{TiO}_2$  films at r.t. although the differences are not significantly large. Nevertheless, higher doping apparently resulted in the decrease of sheet resistance.

In this study, Nb-doped  $\text{TiO}_2$  films were incorporated as HBL in OSC single cells as schematically shown in Fig. 5(a), and the power performance of each cell was tested. To be used as HBL, a film should be thin enough to facilitate electron passage while it should be free from pin hole in order to block the hole transport. Otherwise, charge recombination can happen to deteriorate the cell efficiency. The film coating procedure of HBL was practically the same as that on Si wafer used for

surface morphology characterization, while the concentrations and coating rates were modified to get thinner films. In Table 3, solar cell performances of the single cells with undoped and Nb-doped  $\text{TiO}_2$  HBL layers are summarized. The values in Table 3 have been averaged from two independent experiments for all three cases. It was confirmed that Nb-doped HBLs show higher  $J_{sc}$  and PCE than those with undoped  $\text{TiO}_2$ . We can suggest two reasons for the enhanced PCE. First, smaller particle size due to Nb-doping may have resulted in a formation of better interlayer. Compared to large particles, a smaller nanoparticle enables much more uniform and pinhole-free HBL layer through which hole transport can be effectively blocked. Taking into account a comparable or slightly higher sheet resistance of the Nb-doped  $\text{TiO}_2$  films than an undoped film, enhancement of PCE as shown in Fig. 5(b) is noteworthy. The reason can be attributed to other parameters such as carrier concentration and electron mobility within the film which could affect higher photocurrent generation through Nb-doped  $\text{TiO}_2$  HBL films. Upon exposure to solar radiation, interfacial resistance between active layer and electrode is supposed to be reduced, which resulted in the enhancement of fill factor (FF) of the solar cells [27]. In this regard, Nb-doped  $\text{TiO}_2$  nanoparticles higher than 6% with an improved dispersibility in organic solvent are called for toward higher power conversion performance in OSC by further optimizations both in the particle synthesis and the fabrication process of HBL film.

#### 4. Conclusion

Via sol–gel route, we synthesized Nb-doped  $\text{TiO}_2$  nanoparticles, with doping rates up to 6 mol%. The size of nanoparticles ranging from 1.8 to 2.4 nm and anatase crystalline phase was characterized by XRD. All the samples were well dispersed in alcohol solvent due to organic ligands attached to  $\text{TiO}_2$  nanoparticles, and thus uniform thin films with subnanometer scale roughness could be obtained. Ellipsometry analyses on thin films revealed that the refractive indices were increased by ~20% by thermal sintering. Uniform thin films of Nb-doped  $\text{TiO}_2$  nanoparticles were utilized as HBL of OSC, and improved PCE by Nb doping was confirmed by single cell performance measurements.

#### Acknowledgments

Authors thank H. Park in Kookmin University for measuring film resistance. W. Lee gratefully acknowledges the support by the Center for Electro-Photo Behaviors in Advanced Molecular Systems at POSTECH (No. 2012-0000532). K. Kim acknowledges the New & Renewable Energy of the Korea Institute of Energy Technology Evaluation and Planning (KETEP) grant funded by the Korea Government Ministry of Knowledge Economy (2012T100100054). H. Lee acknowledges the financial support by the National Research Foundation of Korea grant funded by the Korean Government (MEST) (NRF-2012R1A2A2A01014288).

Table 3  
OSC performance data of single cells with Nb-doped  $\text{TiO}_2$  as HBL.

HBL	$V_{oc}$ (V)	$J_{sc}$ ( $\text{mA}/\text{cm}^2$ )	FF	Efficiency
Bare $\text{TiO}_2$ HBL	$0.64 \pm 0.00$	$8.40 \pm 0.03$	$0.50 \pm 0.01$	$2.66 \pm 0.06$
3% Nb- $\text{TiO}_2$ HBL	$0.64 \pm 0.01$	$8.62 \pm 0.23$	$0.52 \pm 0.02$	$2.81 \pm 0.21$
6% Nb- $\text{TiO}_2$ HBL	$0.63 \pm 0.01$	$8.90 \pm 0.29$	$0.67 \pm 0.02$	$3.76 \pm 0.22$

## References

- [1] O. Morton, *Nature* 443 (2006) 19.
- [2] K.M. Coakley, Y.X. Liu, C. Goh, M.D. McGehee, *MRS Bull.* 30 (2005) 37.
- [3] G. Dennler, C. Lungenschmied, H. Neugebauer, N.S. Sariciftci, A. Labouret, *J. Mater. Res.* 20 (2005) 3224.
- [4] S.E. Gledhill, B. Scott, B.A. Gregg, *J. Mater. Res.* 20 (2005) 3167.
- [5] M. Gratzel, *MRS Bull.* 30 (2005) 23.
- [6] S. Gunes, H. Neugebauer, N.S. Sariciftci, *Chem. Rev.* 107 (2007) 1324.
- [7] M. Lira-Cantu, F.C. Krebs, *Recent Res. Dev. Appl. Phys.* 8 (2005) 71.
- [8] S.E. Shaheen, D.S. Ginley, G.E. Jabbour, *MRS Bull.* 30 (2005) 10.
- [9] D. Heithecker, A. Kammoun, T. Dobbertin, T. Riedl, E. Becker, D. Metzendorf, D. Schneider, H.H. Johannes, W. Kowalsky, *Appl. Phys. Lett.* 82 (2003) 4178.
- [10] P. Peumans, S. Uchida, S.R. Forrest, *Nature* 425 (2003) 158.
- [11] B. Clafin, D.C. Look, *J. Vac. Sci. Technol. B* 27 (2009) 1722.
- [12] A.V. Emeline, Y. Furubayashi, X.T. Zhang, M. Jin, T. Murakami, A. Fujishima, *J. Phys. Chem. B* 109 (2005) 24441.
- [13] Y. Furubayashi, T. Hitosugi, T. Hasegawa, *Appl. Phys. Lett.* 88 (2006).
- [14] R. Ghosh, S. Mridha, D. Basak, *J. Mater. Sci.—Mater. Electron.* 20 (2009) 371.
- [15] M. Hirano, K. Matsushima, *J. Am. Chem. Soc.* 89 (2006) 110.
- [16] A. Kubacka, G. Colon, M. Fernandez-Garcia, *Catal. Today* 143 (2009) 286.
- [17] A. Mattsson, M. Leideborg, K. Larsson, G. Westin, L. Osterlund, *J. Phys. Chem. C* 110 (2006) 1210.
- [18] T. Miyagi, M. Kamei, I. Sakaguchi, T. Mitsuhashi, A. Yamazaki, *Jpn. J. Appl. Phys., Part 1* 43 (2004) 775.
- [19] N. Serpone, *J. Phys. Chem. B* 110 (2006) 24287.
- [20] A. Zaleska, *Recent Patents Eng.* 2 (2008) 157.
- [21] S.X. Zhang, D.C. Kundaliya, W. Yu, S. Dhar, S.Y. Young, L.G. Salamanca-Riba, S.B. Ogale, R.D. Vispute, T. Venkatesan, *J. Appl. Phys.* 102 (2007) 013701.
- [22] W.S. Chung, H. Lee, W. Lee, M.J. Ko, N.G. Park, B.K. Ju, K. Kim, *Org. Electron.* 11 (2010) 521.
- [23] X. Zhang, F. Liu, Q. Huang, G. Zhou, Z. Wang, *J. Phys. Chem. C* 115 (2011) 12665.
- [24] Y.G. Seo, M.A. Kim, H. Lee, W. Lee, *Sol. Energy Mater. Sol. Cells* 95 (2011) 332.
- [25] A.M. Ruiz, G. Dezanneau, J. Arbiol, A. Cornet, J.R. Morante, *Chem. Mater.* 16 (2004) 862.
- [26] M.Z. Atashbar, H.T. Sun, B. Gong, W. Wlodarski, R. Lamb, *Thin Solid Films* 326 (1998) 238.
- [27] S. Lee, J.H. Noh, H.S. Han, D.K. Yim, D.H. Kim, *J. Phys. Chem. C* 113 (2009) 6878.